Desalination and Water Treatment
www.deswater.com

doi: 10.5004/dwt.2022.28134

249 (2022) 232–245
February

Characterization, efficiency, and mechanism in removing heavy metals by a mixed biochar derived from sludge and banana peel

Ying Fu[a,*], Shucong Hua[b], Yanting Yang[c], Sibao Yang[c], You Zhang[c], Genyuan Zhang[a]

[a]*School of Civil Engineering and Architecture, University of Jinan, Shandong, Jinan 250022, China, Tel. +(86)15863798335; emails: cea_fuy@ujn.edu.cn (Y. Fu), zhanggy_tmjzxy@163.com (G.Y. Zhang)*
[b]*Shandong Provincial Architectural Design & Research Institute Co., Ltd., Shandong, Jinan 250001, China, email: huasc_tmjzxy@163.com (S.C. Hua)*
[c]*Shuifa Technology Group Co., Ltd., 30, Huayang Rode, Shandong, Jinan 250199, China, emails: yyt_141210@163.com (Y.T. Yang), yangsb_shuifagh@163.com (S.B. Yang), 401097449@qq.com (Y. Zhang)*

Received 21 August 2021; Accepted 2 January 2022

ABSTRACT

A mixed waste biochar (MWBC), banana peel biochar (BPBC) and sludge biochar (SBC) were made using banana peel and sludge, and were characterized with Brunauer–Emmett–Teller, scanning electron microscopy, Fourier-transform infrared spectroscopy, and Zeta Potential Analyzer, respectively. Some MWBC was leached with HCl to prepare an acid-leaching MWBC (H-MWBC), and the changes in characteristics of MWBC and H-MWBC before and after adsorbing heavy metals (Pb(II), Cu(II) and Zn(II)) were also investigated. The adsorption performance and adsorption kinetics for the above heavy metals were probed with atomic absorption spectrometer, and adsorption mechanism was simply revealed. The results showed that MWBC negatively charged gave a large specific surface area with almost no microporous structures. MWBC was a complex combination of sludge and banana peel, instead of simple mixing of SBC and BPBC, in which the contribution of banana peel was not in porous structure, but in other types of surface area. The suitable pH of the test waters for MWBC to adsorb Pb(II), Cu(II) and Zn(II) were 2, 4, and 4, and adsorption capacity were 40.1,40 and 39.6 mg/g at dosage 5 g/L, respectively, all reaching 100% adsorption efficiency. The adsorption rate of MWBC for heavy metal ions was Cu(II) > Zn(II) > Pb(II), and MWBC gave a stronger temperature sensitivity to Pb(II) than Cu(II) and Zn(II) and can be used in wider concentration ranges for Pb(II) and Cu(II). MWBC gave much higher adsorption performance for metals than H-MWBC, and posed higher Cu(II) adsorption performance than BPBC and SBC. The adsorption process of MWBC for Pb(II), Cu(II), and Zn(II) was in accordance with the pseudo-second-order kinetic process. Probably having both hydrophilic and hydrophobic natures, MWBC mainly exhibited non-porous adsorption, in which the mechanism was dominated by chemical adsorption of electrostatic neutralization/adsorption, assisted by physical adsorption, while the physical adsorption was dominant in H-MWBC.

Keywords: Sewage sludge; Banana peel; Biochar; Heavy metals

* Corresponding author.

1. Introduction

Since the last century, desertification has been devouring the land terribly [1,2], and desertification and drought almost make at least 12 million ha of land lost every year, causing agricultural land increasingly barren. In addition, the global heavy metal pollution is becoming more and more prominent with the development of global economy [3–5], further worsening the usability of arable land. The metals which are released into waters or soils are generally originated from human and industrial activities [6]. Especially, the heavy metal pollution coexisting in various forms in water and soil environment has shown an increasing trend of superposition with the accelerating of both urbanization and industry and agriculture development in China during the half past decades [7]. These metals are difficult to remove due to their high solubility [6]. After entering the human body through food chain, the heavy metals exceeding a certain threshold will cause some irreversible harm to the human digestive system, nervous system, bone marrow hematopoietic system, or other organs [8,9].

At present, adsorption is one of the techniques to remove heavy metals from water and wastewater [10–12]. Generally, adsorbents mainly include inorganics (zeolites, diatomite, attapulgite, bentonite, etc), organics (cellulose, chitosan, starch, etc.), biologicals (bacteria, fungi, agricultural and forestry wastes), and carbonaceous materials (activated carbon, graphene oxide, biochar, etc.) [13,14]. As a new sort of eco-friendly adsorbent which is a kind of solid product during pyrolysis processes [15], biochar (BC) has been a research hotspot for a long time [16,17]. The modified BC was characterized by having unique aromatic structure, large surface area with much pore structures and rich functional groups (improving stability), and high adsorption efficiency and ion exchange capacity [9,18,19]. In recent years, the application of BC in agriculture, environment, and energy has aroused more and more attention [11,20–24], in which the removal of heavy metals (involving Pb^{2+}, Zn^{2+}, Cd^{2+}, Cu^{2+}, Ni^{2+}, As^{5+}, Cr^{3+}, Cr^{6+}, Hg^{2+}, etc.) has been widely studied [1,11,25–32]. Therefore, Cu^{2+}, Pb^{2+} and Zn^{2+} were selected as removal objects in this work.

A variety of raw materials can be used to prepare BC, including woody biomass, agricultural residues and sewage sludge [33,34], in which much studies were about surplus sludge and agricultural and forestry waste [35–37], however, the preparation of BC using fruit peel [38–40] or using both biomass and sewage sludge [33,41,42] and the removal of heavy metals with this kind of BC were worth studying further.

The yield of banana and plantain in the world was estimated to reach more than 1.5×10^8 tons in 2018 [43], and the total banana output reached 11.22 million tons in 2018 in China. Generally, the peel of banana accounts for around 30%–50% of the total weight of banana [43,44]. In addition, according to China Statistical Yearbook of Urban Construction from 1978 to 2018, the total amount of dry sludge in China reached around 10.54 million tons in 2017. With the economy development and improvement of people's living standards, the output of banana peel and sludge increase rapidly, causing a huge crisis to the environment. The main components of banana peel include pectin, cellulose, hemicellulose, lignin, etc., and there were many active groups in these components having a large amount of hydroxyl and carboxyl which can be combined with pollutants in water and soil by various actions, such as chelating, coordinating, complexing and hydroxyl bonding, etc. So the banana peel has great value in eliminating pollutants. As for the preparation of BC using sewage sludge, there were lots of studies have been conducted for a long time [45–47].

Based on the current large output of both banana peel and sludge and their harm to the environment, the research on BC preparation from these two wastes is more realistic, and also is one of important methods in removing pollutants from water and soil. In the BC preparation, most substances can be utilized fully: cellulose, polysaccharide, lignin and other components in the peel of banana, and the carbonaceous and other elements and heat value in the sewage sludge, deserving further study with great application value. At present, extensive research is being carried out on banana peel in various fields worldwide, involving adsorption [48–50], coagulation [51–53], renewable energy [43,54], etc. As for the sludge, more and more application research is being developed in the field of water and wastewater treatment [46–55]. The banana peel and sewage sludge were used as raw materials to prepare BC in this work due to their abundance and low cost.

In this work, banana peel biochar (BPBC), sludge biochar (SBC) and mixed waste biochar (MWBC) were prepared using the peel of banana and sewage sludge, and some MWBC were leached by HCl to make an acid-leached MWBC (H-MWBC). Then the characteristics of MWBC was studied with Brunauer–Emmett–Teller (BET), scanning electron microscopy (SEM), Fourier-transform infrared spectroscopy (FTIR), and zeta potential, respectively, compared with that of SBC and BPBC, and the difference of characteristics between MWBC and H-MWBC before and after adsorbing heavy metals (Pb(II), Cu(II) and Zn(II)) was also studied. And then the adsorption performance and adsorption kinetics of MWBC for the above heavy metals were probed with atomic absorption spectrometer, and adsorption mechanism was also analyzed. This work explores a feasible and realistic way for the recycling of the two solid wastes and the developing of comprehensive biochars.

2. Materials and methods

2.1. Preparation of BC

2.1.1. Preparation of MWBC, SBC, BPBC and H-MWBC [56]

Some dry banana peel (Hainan, China) and sewage sludge (Jinan, China) were obtained after natural drying in sunshine for 72 h, respectively, and then were further dried in oven for 12 h at 105°C by GZX-9140MBE Electric Heat Forced Air Drying Oven (Shanghai Boxun, China). After that, they were smashed with CS-700 COSUAI High Speed Multi-function Pulverizer (Zhejiang, China) to make peel powder and sludge powder, respectively. Finally, the peel powder and sludge powder passed through the mesh screen with 100 mesh to obtain the sifted materials, respectively.

Preparation of MWBC. The peel powder and sludge powder were mixed up at a ratio of 1:1, and then was pyrolyzed in SX2-8-16 High Temperature Box Resistance Furnace

(Longkou Electric Furnace Factory, China) with the following conditions: heating rate was 15°C/min, and final temperature was controlled 400°C for 120 min. A black granular MWBC was obtained, and then was crushed and sealed.

Preparation of SBC and BPBC. The peel powder and sludge powder were respectively pyrolyzed under the same conditions as MWBC. A black granular SBC and BPBC were obtained, and then were crushed and sealed, respectively.

Preparation of H-MWBC. 0.4 L HCl solution (1 mol/L, analytical grade) was introduced rapidly into 2 g MWBC under medium stirring for 24 h at room temperature, followed by several times of rinsing to make the pH of rinsing water stable, and was then filtrated and dried. A black granular H-MWBC was obtained, and then was crushed and sealed.

2.1.2. Preparation of MWBC and H-MWBC after adsorbing heavy metals

The three test water samples of heavy metals (Pb(II), Cu(II) or Zn(II)) were made as follows, respectively. 1.599 g $PbNO_3$ or 3.969 g $CuSO_2{\cdot}5H_2O$ was dissolved in a certain amount of deionized water under stirring, respectively, in which 10 mL HNO_3 solution ($w(HNO_3)$ = 65%–68%, analytical grade) was added to $PbNO_3$ solution. After that, the $PbNO_3$ or $CuSO_2$ solution was adjusted to 1,000 mL to obtain the Pb(II) stock solution and Cu(II) stock solution, respectively. 1 g solid zinc (w(Zn) = 99.9%) was dissolved in 50 mL HCl solution (2 mol/L, analytical grade), and then was adjusted to 1,000 mL to obtain a Zn(II) stock solution. A certain amount of the three stock solutions were diluted to 200 ± 5 mg/L as the initial concentrations, and then the pH was respectively adjusted to 1.97–2.04, 4.01–4.05 and 4.01–4.05 (determined according to the relevant test results) using HCl solution (w(HCl) = 36%, analytical grade) or NaOH solution (2 mol/L, analytical grade), used as the test water samples.

Six 250 mL conical flasks were used for the adsorption tests, in which the three for MWBC, and the other three for H-MWBC. In the adsorption tests, 100 mL of the test water samples were first introduced into the conical flasks, respectively. And then a certain dosage of MWBC and H-MWBC were respectively added to the test water samples for the adsorption tests which were carried out on SPX-250B-D constant temperature culture oscillation chamber (Changzhou Guowang). The dosage of MWBC and H-MWBC in each flask was selected as 5 g/L according to the relevant test results in the following section 3.2.1. And the adsorption temperature, oscillator frequency and adsorption time were selected as 25°C, 160 rad/min and 120 min, respectively. After the adsorption processes, the vacuum filtration was conducted for each sample, and then each filtration residue was rinsed three times with deionized water, respectively. And then each filtration residue rinsed was dried in GZX-9140 MBE Electric Heat Forced Air Drying Oven (Shanghai Boxun, China) for 12 h at 105°C and passed through mesh screen with 200 meshes to obtain the "MWBC or H-MWBC after adsorbing heavy metals", respectively, and finally sealed after crushed. The "MWBC after adsorbing heavy metals" was recorded as MWBC + Pb(II), MWBC + Cu(II), and MWBC + Zn(II) and the "H-MWBC after adsorbing heavy metals" was recorded as H-MWBC + Pb(II), H-MWBC + Cu(II) and H-MWBC + Zn(II), respectively.

2.2. Characterization of BC

2.2.1. Specific surface area and pore structure with BET method

V-Sorb 2800P BET Analyzer (Beijing Jinaipu Technology Co., Ltd., China) was used to analyze the specific surface area and pore structure of MWBC, SBC and BPBC, in which varies porous area and distribution, volume and distribution, and adsorption capacity were analyzed with single-point/multi-point BET, T-graph and Barrett–Joyner–Halenda (BJH) methods, respectively.

2.2.2. Functional groups with FTIR method

The FTIR spectra of MWBC, SBC, BPBC, and H-MWBC were analyzed with Nicolet IS10 Fourier Transform Infrared Spectrometer (Nicolet, USA) under 10 MPa, and 400–4,000 cm^{-1} with a resolution of 4 cm^{-1}. And the FTIR spectra of MWBC and H-MWBC after adsorbing heavy metals (Pb(II), Cu(II) and Zn(II)) were also studied, in which the adsorption tests were the same as Section 2.1.2. Three runs were performed, and the results represented the averages of the tests.

2.2.3. Surface morphology with SEM method

The surface morphology of MWBC, SBC, BPBC, and H-MWBC were analyzed by QUANTA FEG 250 Field emission Scanning Electron Microscope (FEI, USA) at 10,000 (scale bar of 5 μm) times magnification, 10 kV accelerating voltage and 5 nm resolution, respectively. And the surface morphology of MWBC and H-MWBC after adsorbing heavy metals (Pb(II), Cu(II) and Zn(II)) were also studied, in which the adsorption test was the same as Section 2.1.2 – Preparation of MWBC and H-MWBC after adsorbing heavy metals.

2.2.4. Characteristics of charge with zeta potential method

Some MWBC, SBC, BPBC, and H-MWBC were passed through the mesh screen with 200 mesh to obtain sifted materials, respectively. 5 g sifted materials of the above BC were added to 100 mL deionized water and then put in KQ-500DE CNC Ultrasonic Cleaner (Shanghai Suiou, China) for dispersing 30 min, respectively. And then a Zetasize Nano ZS 90 Malvern Laser Particle Size Analyzer (Malvern, UK) was used to analyze the zeta potential of the dispersing samples. Likewise, the zeta potential of MWBC and H-MWBC after adsorbing heavy metals (Pb(II), Cu(II) and Zn(II)) were also studied using the same method. Each sample was measured 3 times in parallel, and the results represented the averages of the tests.

2.3. Adsorption behavior of BC for heavy metals with atomic absorption method

Both the test water samples and adsorption tests were the same as Section 2.1.2 – Preparation of MWBC and

H-MWBC after adsorbing heavy metals, in which the initial concentrations of Pb(II), Cu(II), and Zn(II) were all 200 ± 20 mg/L, the pH was 1.97–2.04 for Pb(II), and 4.01–4.05 for both Cu(II) and Zn(II).

After the adsorption processes, a certain amount of samples were taken out and were allowed to stand for 3–5 min, and followed by a filtration with a 0.45 μm filter membrane to obtain Pb(II), Cu(II), and Zn(II) filtrates, respectively. Pb(II), Cu(II), and Zn(II) concentrations in the filtrates were measured with TAS-990 Atomic Absorption Spectrophotometer (Beijing General Instruments, China), respectively. Finally, the adsorption efficiency was calculated according to the difference of the heavy metal levels before and after adsorption processes, and the adsorption capacity was calculated according to the concentration difference and dosage. Each sample was measured three times in parallel, and the results represented the averages of the tests.

2.3.1. Influence of adsorption factors on MWBC adsorption behavior for heavy metals

The factors mainly included the pH values of test water samples, adsorption time, MWBC dosage, adsorption temperature and heavy metal concentrations, in which the MWBC dosage was selected as 5 g/L except for the test of "dosage", and the adsorption temperature was selected as 25°C except for the test of "adsorption temperature".

The pH values of test water samples: the pH values were from 1.7 to 6, and the adsorption time was selected as 24 h.

Adsorption time: the adsorption time was from 0 to 480 min.

Dosage: the dosage of MWBC was from 1 to 9 g/L, and the adsorption time was selected as 120 min.

Adsorption temperature: the adsorption temperature was from 10°C to 50°C, and the adsorption time was selected as 120 min.

Initial concentration of heavy metals: the initial concentration of Pb(II), Cu(II), and Zn(II) were all from 10 to 500 mg/L, the adsorption time was selected to be 120 min, and the MWBC dosage was selected to be 5 or 7 g/L, respectively.

2.3.2. Adsorption behavior of MWBC, SBC, BPBC and H-MWBC for heavy metals

The adsorption temperature and adsorption time were selected as 25°C and 120 min, respectively.

Comparison of adsorption performance between MWBC, SBC and BPBC: Cu(II) was selected as the metal ion, and the dosage was from 1 to 9 g/L.

Comparison of adsorption performance between MWBC and H-MWBC: The dosage was selected as 5 g/L, and the adsorption time was set to be 120 min.

2.4. Adsorption kinetics of MWBC for heavy metals

According to the test results in Section 2.3.1 – Influence of adsorption factors on MWBC adsorption behavior for heavy metals, the linear fitting processes of MWBC adsorption for the above heavy metal ions were carried out by using the pseudo-first-order kinetic Eq. (1) and pseudo-second-order kinetic Eq. (2) [57], respectively.

$$\ln\left(Q_m - Q_t\right) = \ln Q_m - K_1 t \tag{1}$$

$$\frac{t}{Q_t} = \frac{1}{K_2 Q_m^2} + \frac{t}{Q_m} \tag{2}$$

where K_1 and K_2 are the pseudo-first-order and pseudo-second-order adsorption rate constants, t is the adsorption time, and Q_t and Q_m are the adsorption capacity at t and equilibrium states, respectively. During the linear fitting processes, t was used as the abscissa for Eqs. (1) and (2), and $\ln(Q_m - Q_t)$ and t/Q_t were used as the ordinates in Eqs. (1) and (2), respectively.

3. Results and discussion

3.1. Characterization of BC

3.1.1. Specific surface area and porous structure

The relevant results obtained from the BET analysis of MWBC, SBC, and BPBC are summarized in Table 1. The specific surface area of MWBC was basically equivalent to the sum of the surface area of SBC and BPBC, and was almost 2.36 times that of SBC and 1.60 times that of BPBC, respectively. MWBC and BPBC almost gave no micropore structures, and SBC had a little micropore structures. The total pore volume, adsorption or desorption volume of MWBC was almost similar to that of BPBC, but smaller than that of SBC. As displayed in Table 1, MWBC posed much smaller average pore diameter than SBC or BPBC, but had similar adsorption/desorption pore diameter to BPBC or SBC. Therefore, it can be preliminarily estimated that MWBC's adsorption for heavy metals maybe mainly relies on the adsorption sites on its larger surface area, while only assisted by the adsorption of pore structures, which was consistent with the saturated adsorption amount of the multi-point BET single layer (Table 1), and also with the following test results about characterization (Figs. 1–3) or adsorption behavior (Figs. 4–6).

3.1.2. Functional groups

Fig. 1 presents the comparison of FTIR spectra between MWBC, H-MWBC, SBC and BPBC (Fig. 1a), and between MWBC and H-MWBC before and after adsorbing heavy metals (Fig. 1b and c). To make the changes in the FTIR spectra of BC before and after adsorbing heavy metals clearer, the FTIR spectra of both MWBC and H-MWBC before adsorbing heavy metals were also displayed again in Fig. 1b and c.

As shown in Fig. 1, MWBC appeared to be a kind of typical aromatic ring characteristics consisting of a series of peaks of 3,412–3,455 cm^{-1}, 1,421–1,443 cm^{-1}, 693–878 cm^{-1}, and 1,622–1,623 cm^{-1}. Generally, BC changes from soft materials to hard substance during its preparation process. During this process, the alkalinity of carbonaceous substance and the amount of both ash and carbon-type substance will increase, and the aromatic properties will be enhanced, what's more, the addition of the banana peel (as one type of biomass) reinforced the aromatic properties [58–60].

Table 1
Comparison of specific surface area, pore volume and size between MWBC, SBC and BPBC

Biochar	Multi-point/ single-point BET specific surface area (m^2/g)	*T*-plot micropore specific surface area (m^2/g)	Total pore volume (mL/g)	BJH adsorption/ desorption pore volume (mL/g)	Average pore diameter (nm)	BJH mesopore adsorption/ desorption average pore diameter (nm)	Multi-point BET single-layer saturated adsorption capacity V_m (mL)
MWBC	3.539/3.372	0.00	0.0885	0.0973/0.0961	99.98	31.40/26.28	0.813
SBC	1.497/1.443	0.582	0.1846	0.2159/0.2106	493.3	30.70/31.24	0.344
BPBC	2.208/1.988	0.000	0.0806	0.0919/0.0925	146	31.32/27.93	0.507

MWBC: Mixed waste biochar; SBC: Sludge biochar; BPBC: Banana peel biochar.

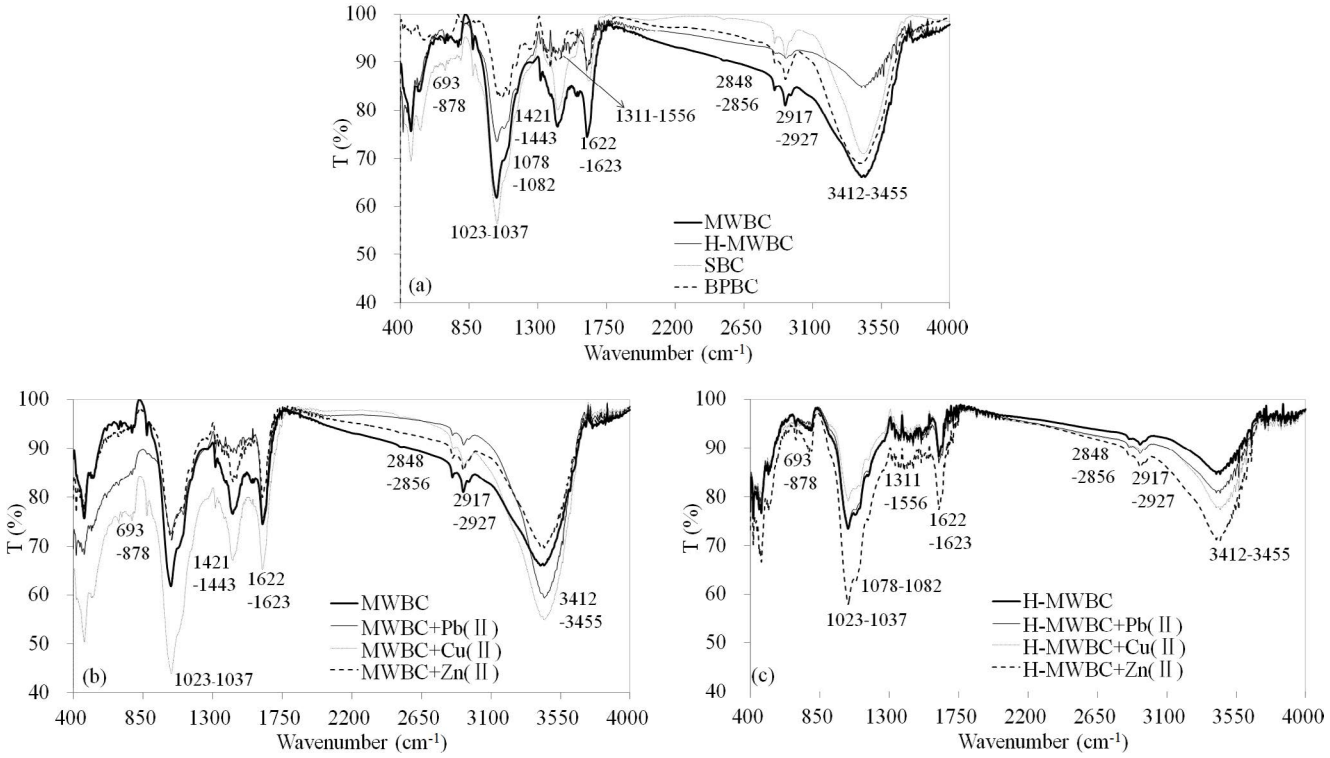

Fig. 1. Comparison of FTIR spectra between (a) MWBC, SBC, BPBC and H-MWBC, (b) MWBC before and after adsorbing heavy metal ions and (c) H-MWBC before and after adsorbing heavy metal ions.

As seen in Fig. 1, the skeleton structure of MWBC was more similar to that of SBC, but, the corresponding relationships of the amount of functional groups between MWBC and BPBC/SBC was complex: some in MWBC were similar to that in SBC, while the others were the superposition of SBC and BPBC. This further inferred that some essential changes occurred in MWBC structures, so MWBC was a complex combination of SBC and BPBC, instead of a simple mixture of the two, which was consistent with the inference in Section 3.1.1.

For H-MWBC, the peak of 1,421–1,443 cm^{-1} disappeared and the intensity of the other peaks were also weakened due to the reaction between acid and some substances in MWBC, weakening the aromatic characteristics. Compared with MWBC, the asymmetry of some both molecules and structures in H-MWBC was weakened, or the number of hydrogen bonds was reduced, but the half-peak width of some individual peaks were slightly increased (such as 1,622–1,623 cm^{-1} and 3,412–3,455 cm^{-1}), that is, the above phenomena occurring at some peaks was a little opposite. In a word, compared with MWBC, the skeleton structure of H-MWBC almost gave no change, but the internal structures and surface properties have changed.

The strong absorption peak at 3,412–3,455 cm^{-1} can be mainly attributed to the stretching vibration of the hydrogen bond formed by hydroxyl group (–OH) on the carbon surface [61,62]. For MWBC, the intensity of 3,412–3,455 cm^{-1} was MWBC + Cu(II) > MWBC + Pb(II) > MWBC > MWBC + Zn(II), and this peak gave a narrower width in "MWBC after adsorbing metals" than in MWBC. This suggested that

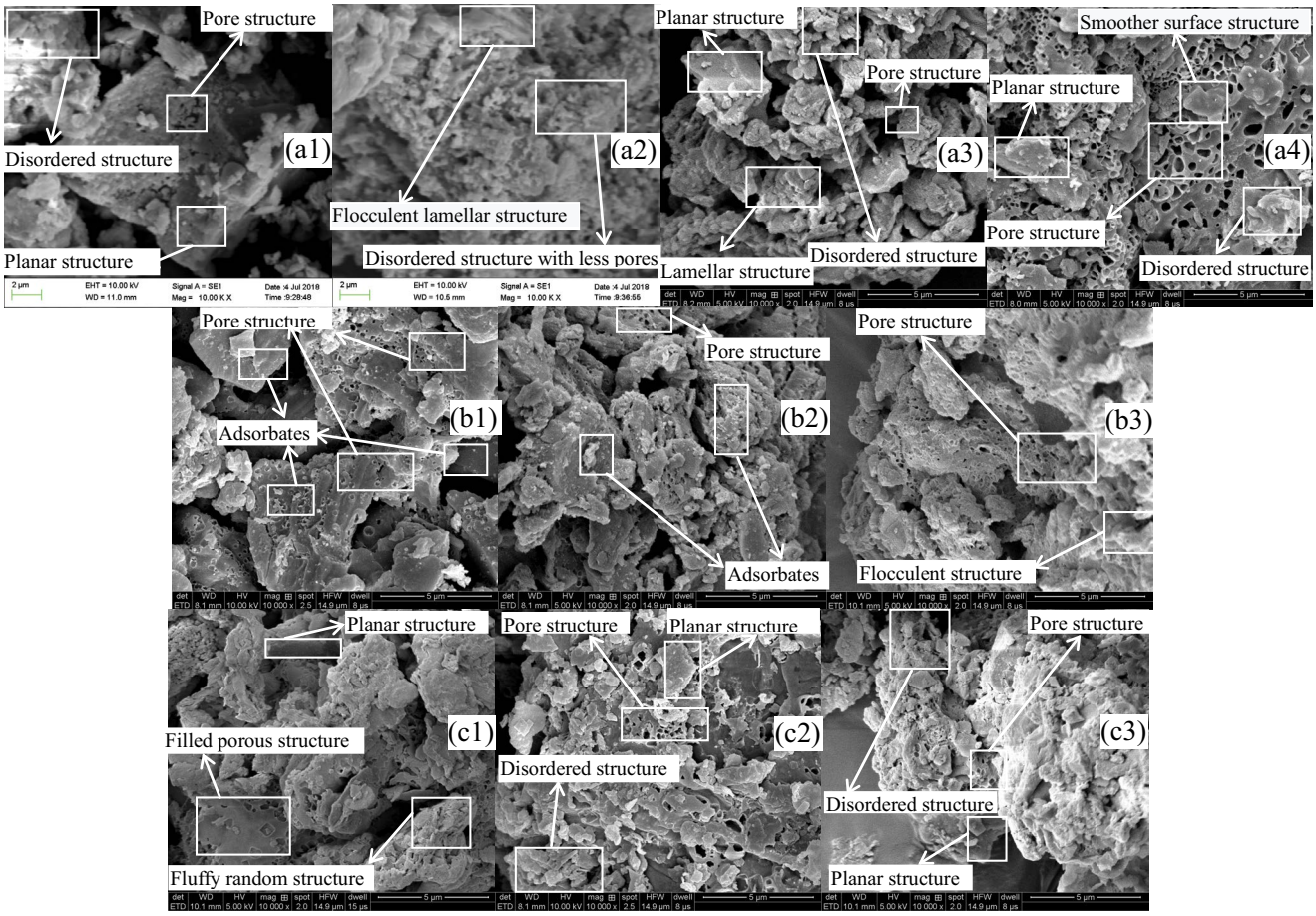

Fig. 2. Comparison of surface morphology between (a) BC (10,000×), (b) MWBC after adsorbing heavy metals (10,000×) and (c) H-MWBC after adsorbing heavy metals (10,000×). (a1) SBC, (a2) BPBC, (a3) MWBC and (a4) H-MWBC; (b1) MWBC + Pb(II), (b2) MWBC + Cu(II) and (b3) MWBC + Zn(II); (c1) H-MWBC + Pb(II), (c2) H-MWBC + Cu(II) and (c3) H-MWBC + Zn(II).

the hydrogen bonds on the carbon surface of MWBC gave the strongest adsorption ability for Zn(II) and the weakest for Cu(II). Moreover, the adsorption of MWBC for Zn(II) almost exceeded the normal adsorption ability of hydrogen bonds, that is, the chemical adsorption may be accompanied by physical adsorption in MWBC. While for H-MWBC, the hydrogen bonds gave the strongest adsorption for Pb(II) and the weakest for Zn(II), moreover, the intensity of the peaks in "H-MWBC after adsorbing metals" were all lower than that in MWBC.

2,848–2,927 cm^{-1} can be assigned to the stretching vibration of C–H or C–CH groups [63]. This bond made some contribution to the adsorption of MWBC for metals, while almost having no any contribution to H-MWBC in absorbing metals. 1,622–1,623 cm^{-1} can be corresponded to the shear vibration of hydroxyl group (–OH). Combined with 1,421~1,443 cm^{-1}, this peak can also be attributed to the vibration absorption peak of C=C skeleton. This peak intensity in MWBC was far greater than that in H-MWBC, indicating that the amount of hydroxy groups on the surface of MWBC was greater than that on H-MWBC. In addition, the peak at 1,622–1,623 cm^{-1} was slightly split in MWBC, indicating that MWBC probably contained some amino bonds ($–NH_2$). For MWBC, the peak intensity of 1,622–1,623 cm^{-1} was MWBC + Cu(II) > MWBC + Pb(II) = MWBC > MWBC + Zn(II), also suggesting that the hydrogen bonds in MWBC gave the strongest adsorption for Zn(II) and the weakest for Cu(II). While for H-MWBC, just like the hydrogen bonds located on the carbon surface, the peak at 1,622–1,623 cm^{-1} gave quite weaker adsorption for Zn(II) and had no adsorption for both Cu(II) and Pb(II), so, there almost had no any change in the intensity of this peak in "H-MWBC before and after adsorbing metal ions". The peaks at 1,421–1,443 cm^{-1} and 1,622–1,623 cm^{-1} may be assigned to the stretching vibration of C–N [61] or to the stretching vibration of C=C skeleton vibrational absorption. The different changes in 3,412–3,455 cm^{-1} and 1,622–1,623 cm^{-1} in both MWBC and H-MWBC after adsorbing metals further indicated that the chemical adsorption of the hydrogen bonds and hydroxyl groups in MWBC was much stronger than that in H-MWBC. Moreover, the hydroxy groups in H-MWBC almost gave no chemical adsorption for Cu(II) and Pb(II), only giving weak absorption for Zn(II).

The peaks at 1,023–1,037 cm^{-1} originated from the stretching vibration of C–O [64] or the characteristic peak of Si–O. The intensity changes in this peak indicated that the C–O bonds in MWBC almost gave the similar adsorption for Zn(II) and Pb(II), all greater than that for Cu(II), while the

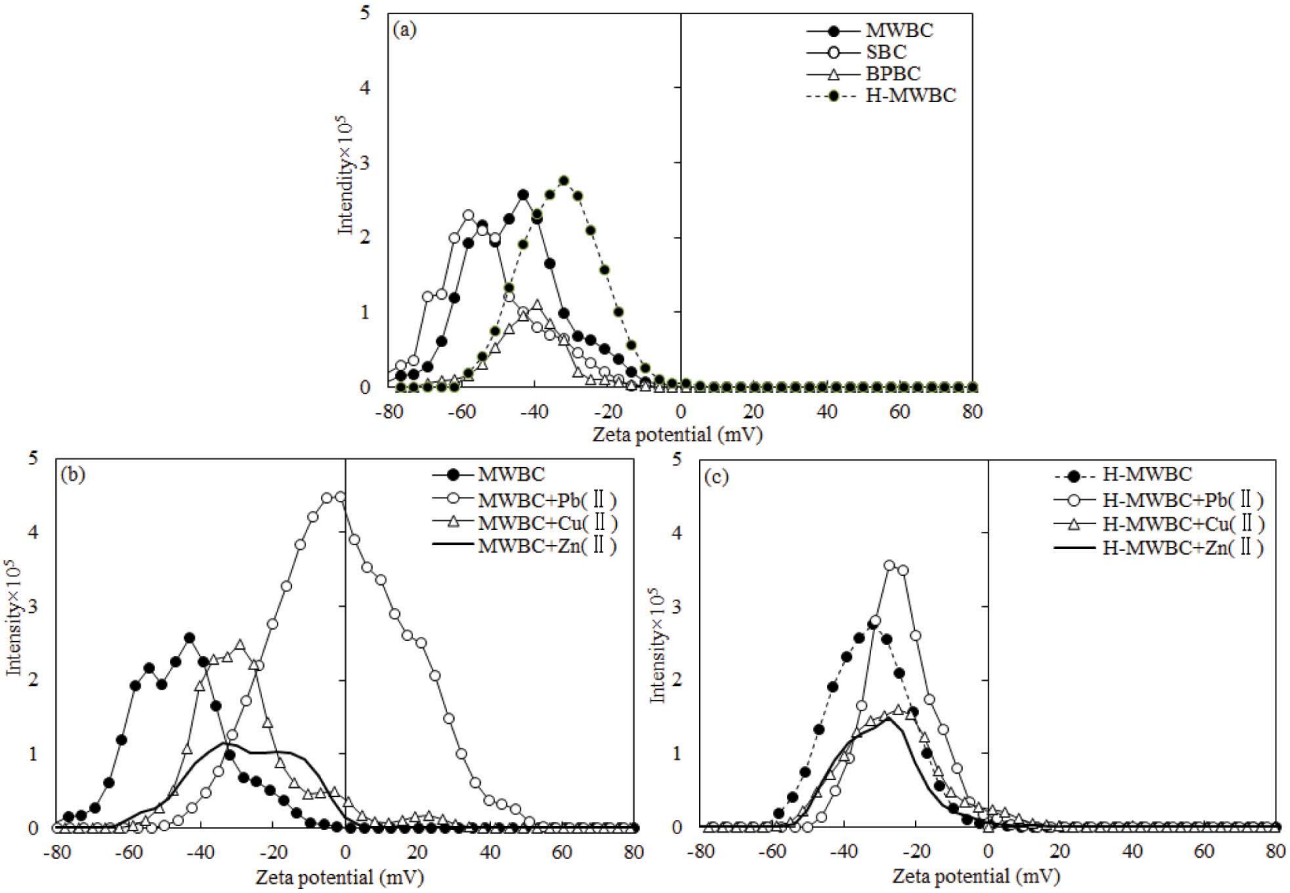

Fig. 3. Comparison of zeta potentials between (a) MWBC, SBC, BPBC and H-MWBC, (b) MWBC before and after adsorbing heavy metal ions, and (c) H-MWBC before and after adsorbing heavy metal ions.

C–O bonds in H-MWBC had the strongest adsorption for Cu(II) and the weakest for Zn(II), almost having no adsorption for Pb(II).

693–878 cm^{-1} can be attributed to the stretching vibration of C–H or out-of-plane bending vibration of C–H in aromatic ring or out-of-plane bending vibration of O–H. For MWBC, this peak appeared to have complex action during adsorbing metal ions. This peak became wider in MWBC + Cu(II), indicating that the number of this peak increased after adsorbing Cu(II), that is, this bond gave some adsorption for Cu(II). This peak almost disappeared after MWBC adsorbing Zn(II) and Pb(II), also indicating that some chemical adsorption occurred, that is, C–H and O–H had adsorption for both Zn(II) and Pb(II). But for H-MWBC, the bond at peak of 693–878 cm^{-1} almost gave no any adsorption for metals.

3.1.3. Surface morphology

Fig. 2 presents the comparison of SEM images among SBC, BPBC, MWBC and H-MWBC (Fig. 2a), and between MWBC (Fig. 2b) and H-MWBC (Fig. 2c) before and after adsorbing heavy metal ions.

Generally, BC is a type of densely packed and twisted structure mainly composed of aromatic sheet. As shown in Fig. 2a, SBC (Fig. 2a1) was mainly composed of a large amount of uniform pore structures, planar-like structures having smaller surface area with less pores, and disordered structures. BPBC (Fig. 2a2) consisted of flocculent lamellar structures having smaller surface area with less pores and fluffy structures having a larger surface area with more pores. Some uniform porous surface in BPBC with diameter which was significantly larger than that in SBC and MWBC were distributed in the above fluffy structures. The surface morphology of MWBC (Fig. 2a3) gave large difference from that of H-MWBC (Fig. 2a4): MWBC (Fig. 2a3) mainly consisted of more disordered structures, less pore structures and sheet structures, and planar structures, in which lots of disordered ditch-like structures with larger diameters were distributed.

However, the surface structure of H-MWBC changed greatly after acid leaching (Fig. 2a4). H-MWBC appeared to be a type of much looser structure consisting of more pore structures with various sizes, less disordered structures and planar-like surface structures. There appeared to be lots of pore structures in H-MWBC, mainly because MWBC was mainly a kind of hydroxyl-based carbon skeleton material (Fig. 1) composed of inorganic, organic substances, ash, etc., so, H^+ reacted with these substances to generate some soluble substances. After the soluble substances entered

to the acid solution (used for acid leaching), a type of network-like carbonaceous structure composed of relatively loose acid-insoluble solids was left. Fig. 2 showed that the surface area of H-MWBC should be much larger than that of MWBC.

After adsorbing Pb(II), Cu(II) or Zn(II), the surface morphology of MWBC was very different from that of H-MWBC. After adsorbing heavy metal ions, MWBC (Fig. 2b) appeared to be a large number of pore structures (Fig. 2b), while lots of pore structures in H-MWBC (Fig. 2c) were filled.

As seen in Fig. 2b, after adsorbing Pb(II), Cu(II) and Zn(II), MWBC gave both similar and different surface morphology characteristics. The similarity was that MWBC + Pb(II), MWBC + Cu(II) and MWBC + Zn(II) all exhibited more porous structures, because the acidity increased during the process of adsorbing heavy metals, which was similar to the acid leaching process (Fig. 2a4). The difference was as follows. The surface morphology of MWBC + Pb(II) appeared to be some pore structures which have been filled or unfilled and some larger planar structures, on which some adsorbates could be clearly observed. The filled pore structures were probably caused by the following two reasons: (1) the pore structures were filled by heavy metal substances, and (2) the acidity of the Pb(II) solution was not enough to completely remove the substances in the pores that could react with the acid or not enough to completely wash away the original ash substances in the pores. The surface morphology of both MWBC + Cu(II) and MWBC + Zn(II) presented to be more porous structures: more adsorbates appeared to be particulate substances in the former and flocculent substances in the latter. While for H-MWBC (Fig. 2c), the surface morphology changed greatly after adsorbing heavy metals, basically was composed of more pore structures (had been filled), disordered structures, less pore structures (unfilled) and less planar structures.

3.1.4. Charged characteristics

Fig. 3 displays the comparison of the change in the charged characteristics between MWBC, SBC, BPBC and H-MWBC (Fig. 3a), and between MWBC (Fig. 3b) and H-MWBC (Fig. 3c) before and after adsorbing heavy metals.

As seen in Fig. 3a, MWBC, SBC and BPBC were all negatively charged. SBC had more negatively charged particles than MWBC and gave slightly lower intensity of negatively charged particles than that of MWBC. BPBC gave less negatively charged particles and lower intensity than MWBC. The amount of negative charges in MWBC was not a simple addition of that of SBC and BPBC. Pb(II), Zn(II) and Cu(II) are positive divalent ions, so, the above-mentioned biochars had electrostatic adsorption for metal ions, thus leading to some reduction of zeta potentials of BC after adsorbing metal ions. As also seen from Fig. 3a, the zeta potential of MWBC was from –80 to –10 mV, almost concentrating around –60 – –40 mV, in which the span of the zeta potential distribution was wider, that is, there were more particles having large negative potential. The zeta potential of H-MWBC was from –60 to –0 mV, almost concentrating around –40 – –20 mV, in which there were less particles having large negative potential. This can be explained as follows. (1) As seen from both FTIR (Fig. 1) and SEM (Fig. 2), MWBC was mainly a type of a hydroxyl-based carbon skeleton material which consisted of inorganic, organic substances, ash, etc., some of which negatively charged (Fig. 3a) reacted with much H^+ in acid solution during the acid leaching process, leading to that the dissolved substances entered into the acid solution and the acid-insoluble substances remained in the carbonaceous solid, causing a right shift of the zeta potential during the changing process from MWBC to H-MWBC. (2) The addition of the banana peel prompted the further formation of network-like structures in H-MWBC (composed of acid-insoluble substances) which was much looser than that in MWBC.

The zeta potential of both MWBC (Fig. 3b) and H-MWBC (Fig. 3c) after adsorbing heavy metals shifted to the right due to the electrostatic neutralization/adsorption, but the right shift amplitude of the former was much larger than that of the latter, suggesting that the electrostatic neutralization/adsorption played a larger role in MWBC for adsorbing heavy metals, which was consistent with the previous analysis (Figs. 1 and 2). For MWBC (Fig. 3b), the right shift amplitude was the largest and the number of the particles charged higher potential was also the greatest after adsorbing Pb(II), but almost giving a similar right shift amplitude in Cu(II) and Zn(II), however, the number of the particles charged higher potential after adsorbing Zn(II) was obviously less than that after adsorbing Cu(II), further suggesting that MWBC gave the strongest chemical adsorption for Zn(II) and the weakest for Cu(II). As also seen in Figs. 3b and c, the number of the particles charged higher potential was MWBC + Pb(II) > MWBC + Zn(II) > MWBC + Cu(II), while basically the same in H-MWBC + Cu(II) as that in H-MWBC + Zn(II). This suggested that the neutralization/adsorption function in H-MWBC for adsorbing heavy metals decreased, and the selectivity in adsorbing heavy metals also reduced, compared with that in MWBC.

3.2. Adsorption behavior of BC for heavy metal ions

3.2.1. Adsorption behavior of MWBC

Fig. 4 shows the impact of different factors (Fig. 4a: pH; Fig. 4b: adsorption time; Fig. 4c: dosage; Fig. 4d: adsorption temperature; Fig. 4e and f: concentration of heavy metal ions, and dosage was 5 g/L in Fig. 4e and 7 g/L in Fig. 4f) on the adsorption behavior of MWBC for Pb(II), Cu(II) and Zn(II), respectively.

PH is closely related to the chemical behavior of aqueous solutions, such as hydrolysis, complexation, precipitation and oxidation of heavy metal ions, and also related to the properties of adsorption sites on biochar surface and the affinity between biochars and heavy metal ions, so pH is one of the important factors influencing the adsorption result and behavior mode of biochars for heavy metal ions.

As seen in Fig. 4a, MWBC had different adsorption behavior for different metal ions within the experimental pH ranges (flocs will be formed if the pH is higher than the values in this experiment). The preferred pH values were 2–4, 4–5 and 4–5 for Pb(II), Cu(II) and Zn(II) respectively, which were consistent with the original pH of the test water samples, so, 2–4, 4–5 and 4–5 were used as the pH values of the following experiments. When the water sample pH

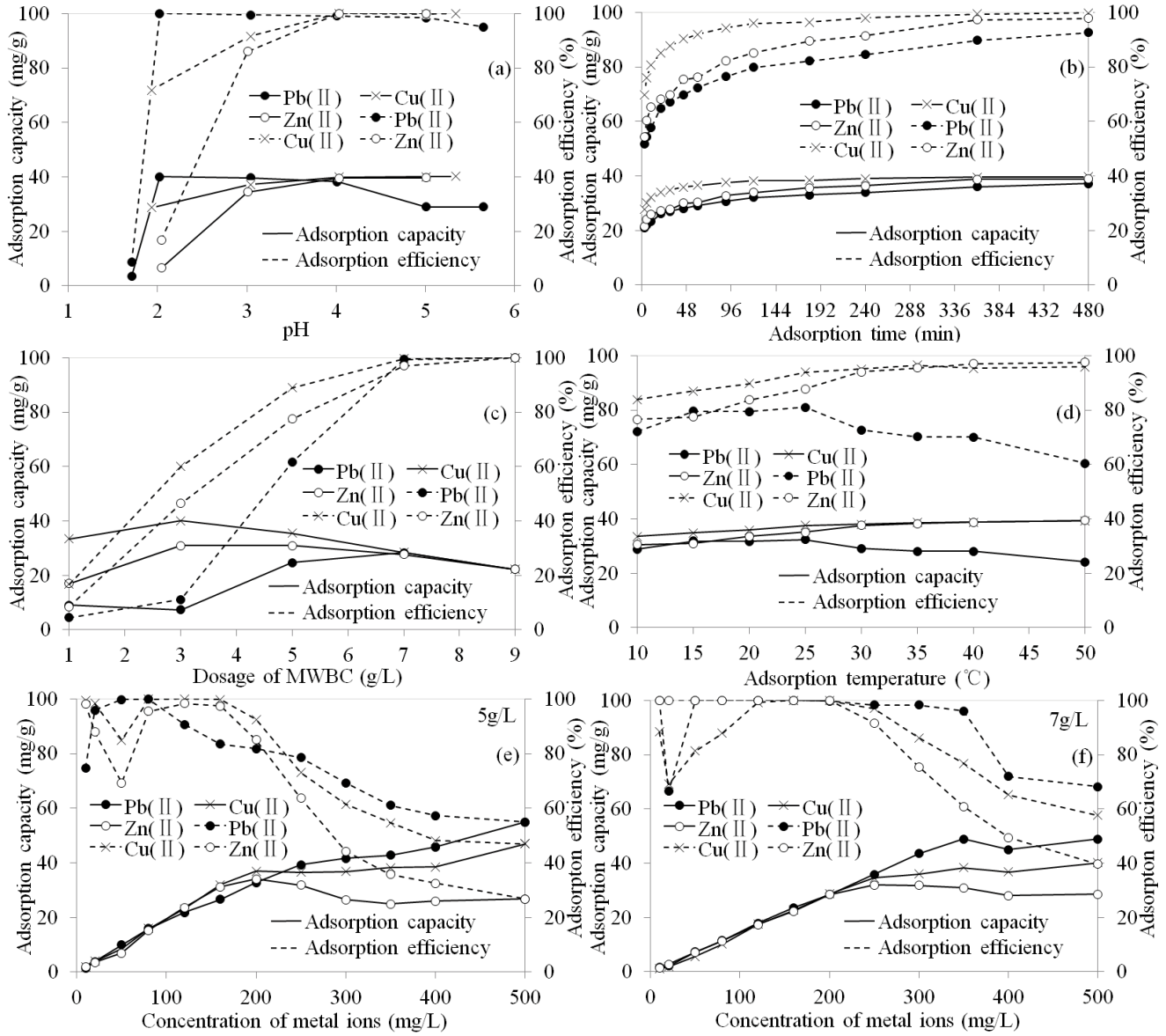

Fig. 4. Impact of (a) pH, (b) adsorption time, (c) dosage, (d) adsorption temperature, (e) concentration of heavy metal ions (dosage = 5 g/L), and (f) concentration of heavy metal ions (dosage = 7 g/L) on adsorption behavior of MWBC for Pb(II), Cu(II) and Zn(II).

changed from the initial lowest values (Fig. 4a: 1.71–2.04) to the preferred values (Fig. 4a: 2, 4 or 4), MWBC gave a larger changes in the adsorption capacity and efficiency for Pb(II) and Zn(II) (the lower the dosage, the greater the change) and a smaller changes for Cu(II), indicating that MWBC adsorption had large sensitivity to the acidity changes in Pb(II) and Zn(II) solutions and a small sensitivity to Cu(II) solution's acidity. When the original pH of the water samples were 2, 4, and 4, the adsorption capacity of MWBC for Pb(II), Cu(II) and Zn(II) were almost the same, with 40.1, 40 and 39.6 mg/g respectively, all the adsorption efficiency almost reaching 100%.

The adsorption capacity of MWBC for Cu(II) and Zn(II) basically remained stable with the increasing of pH, except for Pb(II) (first increased and then decreased). This was because MWBC gave different adsorption mode for different metal ions at different pH. When the pH was at acid side, the heavy metals basically existed as soluble ions, such as Pb^{2+}, Cu^{2+} or Zn^{2+}, respectively. It is generally believed that H^+ was dominant competitively in adsorption process compared with metal ions at this moment [64], resulting in lower adsorption of MWBC for metal ions, which was consistent with the FIIR spectra (Fig. 1a): the surface functional groups were weak base in MWBC, giving stronger adsorption for H^+ having the smallest radius of hydrated ions (R_{H^+} hydration = 2.82) in stronger acidity and giving weaker adsorption for metal ions having larger hydrate ion radius [65]. As the pH increased, the following situation occurred. (1) Protonation reaction occurred on the surface functional groups in MWBC, so, the electronegativity of MWBC was

weakened and the potential density was decreased, thus leading to an increasing of the adsorption for metal ions. The amount of $[Pb(OH)]^+$, $[Cu(OH)]^+$ or $[Zn(OH)_4]^{2-}$ in the water samples increased due to the increase of pH at the same time, leading to an electrostatic complex adsorption of MWBC for $[Pb(OH)]^+$, $[Cu(OH)]^+$ or $[Zn(OH)_4]^{2-}$. (2) MWBC also posed physical adsorption for metal ions: MWBC probably have more macro-porous and trench-like structures having different diameters which were dispersed in its adsorption sites brought about by its larger surface area, which prompted quick transmission of heavy metal ions through the above macro-porous and trench-like structures (Figs. 1 and 2).

As seen in Fig. 4b, the adsorption capacity and efficiency increased with the increasing of adsorption time. For Pb(II), Cu(II) and Zn(II), the adsorption capacity reached 32.1, 38.2 and 33.9 mg/g at 120 min, and 37.1, 39.7 and 38.9 mg/g at 480 min respectively, and the adsorption efficiency reached 79.9%, 95.9% and 85.2% at 120 min, and 92.5%, 99.7% and 97.7% at 480 min respectively. According to the difference of adsorption capacity and efficiency between 120 and 480 min, it could be seen that the adsorption rate of MWBC for metal ions was Cu(II) > Zn(II) > Pb(II), giving the lowest speed for Pb(II) and almost completing the adsorption for Cu(II) within 120 min.

As shown from Fig. 4c, the adsorption efficiency increased with the increasing of dosage, and the adsorption efficiency all reached a stable value of 100% at dosage 7 g/L. The dosage of MWBC was 7, 3 and 3 g/L when reaching the maximum adsorption capacity of 28.4, 40 and 31 mg/g for Pb(II), Cu(II) and Zn(II), respectively, indicating MWBC gave the smallest adsorption capacity for Pb(II) and the largest for Cu(II) at the same dosage. Fig. 4d shows that when the adsorption temperature was lower than 25°C, the adsorption capacity for the three metal ions all increased slightly with the increasing of temperature. When the temperature was higher than 25°C, the adsorption capacity for Pb(II) decreased and for Cu(II) and Zn(II) increased, indicating that MWBC had larger sensitivity to the temperature of Pb(II) solution than that of Cu(II) and Zn(II), and moreover MWBC was not suitable for higher temperature of Pb(II) solution.

As seen from Figs. 4e and f, with increasing the concentration of metal ions, the adsorption efficiency first increased and then decreased, and the adsorption capacity almost increased first and then tended to be stable. For lower concentrations, the adsorption capacity was lower for water samples, consisting with the characteristics of general adsorbents. With the increasing of concentrations, the order of metal ions MWBC gave higher adsorption capacity was Pb(II) > Cu(II) > Zn(II), and the decreasing inflection point of the adsorption efficiency moved backward when MWBC dosage ranged from 5 g/L (Fig. 4e) to 7 g/L (Fig. 4f). Among them, the metal ion concentrations of Pb(II), Cu(II) and Zn(II) at which MWBC gave higher adsorption efficiency moved from 20–80 mg/L (dosage of 5 g/L) to 10 and 50–350 mg/L (dosage of 7 g/L), 10–20 and 80–160 mg/L (5 g/L) to 120–150 mg/L (7 g/L), and 10 and 80–160 mg/L (5 g/L) to 10–200 mg/L (7 g/L), respectively. From the suitable concentration ranges for MWBC to adsorb the three metal ions, Cu(II) had the wider concentration range than Cu(II) and Zn(II) at dosage 5 g/L, while Pb(II) and Cu(II) had the widest and narrowest concentration ranges at dosage 7 g/L, respectively. So, from the adsorption efficiency, Pb(II) concentration range for MWBC to adsorb effectively became wider with the increasing of dosage, while Cu(II) became narrower.

As also seen from Figs. 4e and f, with the increasing of metal concentrations, the metal concentrations at which MWBC began to decrease in adsorption capacity for Pb(II), Zn(II) and Cu(II) was as follows. (1) 5 g/L: none (that is, continuously increasing), none (that is, continuously increasing) and 200 mg /L, respectively. (2) 7 g/L: 350, 350 and 250 mg/L. That is, the maximum adsorption capacities of MWBC for Pb(II), Cu(II) and Zn(II) were 54.9, 47 and 34 mg/g at dosage 5 g/L, 48.9, 40.1 and 32 mg/g at dosage 7 g/L, in which the maximum adsorption capacity for both Pb(II) and Cu(II) occurred at 500 mg/L concentration, while Zn(II) at 200–250 mg/L concentration. Therefore, from adsorption capacity, MWBC can effectively adsorb the narrowest concentration range for Zn(II), but can effectively adsorb a wider concentration range for both Pb(II) and Cu(II). At the same time, the higher dosage of MWBC had negative influence on higher concentration of Pb(II) and Cu(II). So, when MWBC was used to remove Pb(II) and Cu(II), both dosage and metal concentration should be taken into account, while for Zn(II), metal concentration was enough.

3.2.2. Comparison of adsorption behavior between MWBC, SBC, BPBC and H-MWBC

Fig. 5 displays the comparison of adsorption behavior between MWBC, SBC and BPBC for Cu(II) (Fig. 5a), and MWBC and H-MWBC for Pb(II), Cu(II) and Zn(II) (Fig. 5b), respectively.

As seen from Fig. 5a, the adsorption effect of MWBC for Cu(II) was better than that of BC made from the raw materials (SBC or BPBC), respectively, but not a simple addition of SBC and BPBC, further demonstrating that MWBC was not a simple mixing of sludge and banana peel. Compared with MWBC, H-MWBC showed a large decrease in adsorbing Pb(II), Cu(II) and Zn(II), in which the adsorption for Cu(II) reduced the most (with the reduction of adsorption efficiency and capacity of 85.9% and 34 mg/g, respectively) and for Pb(II) dropped the least (with the reduction of 72.5% and 28.7 mg/g, respectively).

3.3. Adsorption dynamic curves of MWBC for heavy metals

Fig. 6 displays the pseudo-first-order (Fig. 6a) and pseudo-second-order (Fig. 6b) adsorption dynamic curves of MWBC for Pb(II), Cu(II) and Zn(II), respectively.

As seen in Fig. 6, for Pb(II), Cu(II) and Zn(II), the linear fitting correlation coefficients of R^2 in the pseudo-second-order kinetic Eq. (2) were 0.9974, 0.998, and 0.9999, respectively, having larger values than that in the pseudo-first-order kinetic of 0.9446, 0.7413 and 0.9692. Therefore, the pseudo-second-order kinetic equation can more accurately fit the adsorption process of MWBC for Pb(II), Cu(II) and Zn(II). At the same time, just as the calculation result from Fig. 6, the equilibrium adsorption capacity (Q_m) of MWBC for Pb(II), Cu(II) and Zn(II) were 13.9, 6.27 and 10.9 mg/g in the pseudo-first-order kinetic Eq. (1) and 36.8, 39.1 and

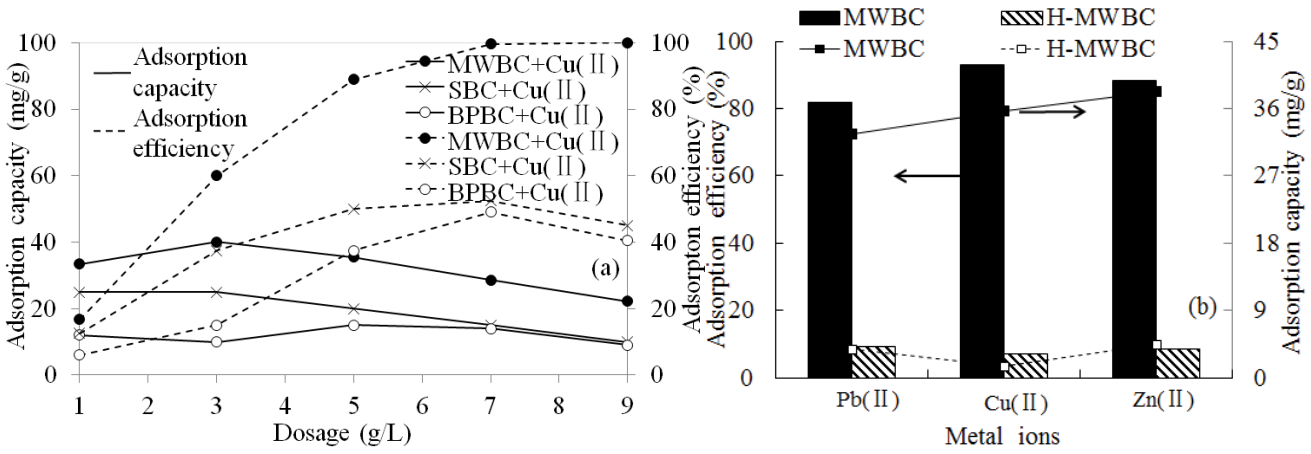

Fig. 5. Comparison of adsorption behavior between (a) MWBC, SBC and BPBC for Cu(II) and (b) MWBC and H-MWBC for Pb(II), Cu(II) and Zn(II). Dosage = 5 g/L.

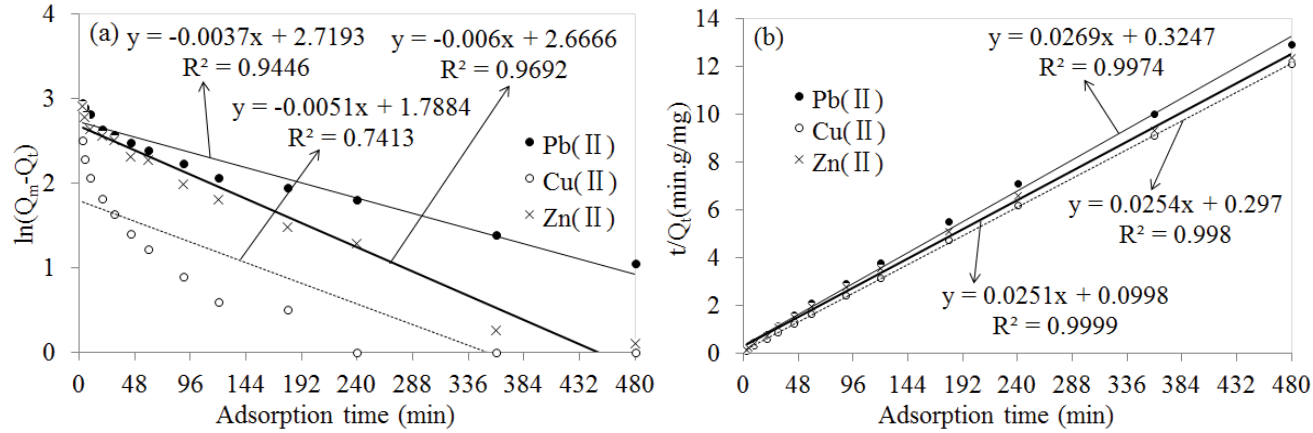

Fig. 6. (a) Pseudo-first-order and (b) pseudo-second-order adsorption dynamic curves of MWBC for Pb(II), Cu(II) and Zn(II). Dosage = 5 g/L.

37.7 mg/g in the pseudo-first-order kinetic Eq. (2), respectively. It can be seen that the fitting values of Q_m in the pseudo-second-order kinetic Eq. (1) were closer to the actual adsorption capacity of 40.1, 40 and 39.6 mg/g (Fig. 4a), indicating that the adsorption of MWBC for Pb(II), Cu(II) and Zn(II) was mainly chemisorption.

3.4. Adsorption mechanism of MWBC for heavy metal ions

From the BET characterization analysis (Table 1), the following inference can be obtained. (1) The banana peel played important role in the other types of surface area in MWBC, instead of pore structures. (2) MWBC was a complex combination of the banana peel and sludge, instead of a simple mixture of the two materials. Furthermore, the structure of MWBC probably has undergone substantial changes during the preparation process from the raw materials.

From the corresponding relationship between the peaks and bond structures in FTIR spectra, it can be inferred as follows. (1) MWBC was a complex combination of the two materials, as inferred in BET results. (2) MWBC surface was composed of –OH, –O, and a small amount of –H, –N, –Si, and –NH_2. MWBC was a type of carbon skeleton stuff which mainly consisted of hydroxyl groups, in other words, MWBC was composed of alkane, lipid, alcohol, phenol, aromatic ring enhancing MWBC stability, amide and a small amount of silicate substances. (3) MWBC displayed a stronger chemical adsorption for metal ions, giving the strongest adsorption for Zn(II) and the weakest adsorption for Cu(II). However, H-MWBC basically did not have chemical adsorption, only showing some physical adsorption.

From the comparison of the changes in the surface morphology between all kinds of BC studied in this work, the following inference could be obtained. (1) The complex reaction of the two materials in MWBC led to the formation of complex and diverse biochar surface structures, lots of which were loosely distributed and three-dimensionally independent, indicating that the surface area of MWBC may be much larger than that of SBC and BPBC. (2) The surface area of H-MWBC should be much larger than that of MWBC, but the latter gave much greater adsorption capacity or efficiency (Fig. 5) for metal ions than the former. This indicated that the disordered structures gave

both larger surface area and more adsorption sites than the pore structures (MWBC performed a type of non-porous adsorption which could be obtained from Table 1), and that most pore structures in MWBC did not play some role in adsorption and MWBC adsorption action mainly derived from both more adsorption sites on its larger surface and rapid transportation process of metals ions through the disordered structures. This further proved that the disordered structures in MWBC gave much higher adsorption efficiency than the pore structures. (3) The pore structures in H-MWBC gave poor adsorption ability for metal ions (according to the following adsorption behavior Fig. 5) because H-MWBC mainly conducted porous adsorption action. The above surface morphology possessed by MWBC was consistent with the properties displayed in Table 1 and Fig. 1.

According to the zeta potential results (Fig. 3), it can be inferred as follows: for positively charged heavy metal ions, H-MWBC will give weakened chemical adsorption and enhanced physical adsorption, which was consistent with the analysis in Figs. 1 and 2.

According to the adsorption effect of MWBC for heavy metal ions (Fig. 5a), there are similarities and differences in adsorption mechanism of MWBC for different metal ions at different pH values, for example, the adsorption mechanism almost included surface electrostatic complexation adsorption, trapping physical adsorption/complexation adsorption, and so on, but having different mechanisms over different acid or base ranges. In addition, the radius of this three hydrate metal ions was Pb^{2+} ($R_{Pb^{2+}\ hydration}$ = 0.265) > Zn^{2+} ($R_{Zn^{2+}\ hydration}$ = 0.216) > Cu^{2+} ($R_{Cu^{2+}\ hydration}$ = 0.206) [65]. As seen from Fig. 4a, the radius of the metal hydrate ions were larger than that of H^+ under strongly acidic conditions (that is, initial pH in this work). So, the ability of surface electrostatic complexation adsorption conducted by MWBC was Cu(II) > Zn(II) > Pb(II), indicating that the adsorption strength of MWBC for the three metal ions was inversely proportional to their hydrated ion radius (that is, the larger the hydrated meal ion radius, the weaker the physical adsorption ability), so, MWBC probably showed some hydrophobic characteristics. However, under weak acid conditions (3 < pH < 5), the surface electrostatic complexation adsorption of MWBC for the three metal ions was almost the same because the radius of the hydrate metal ions were larger than that of H^+, moreover, various forms of metal ions maybe coexisted in water samples, so MWBC was probably a kind of biochar having both hydrophilic and hydrophobic properties. From the result of Fig. 5 and SEM (Fig. 2), it can be further proved that the porous physical adsorption in H-MWBC was much lower than the chemical adsorption in MWBC (caused by the non-porous structures), which was further consistent with the above analysis: banana peel gave positive effect on the adsorption behavior of MWBC although banana peel did not play important role in increasing the porous surface area in MWBC.

In summary, based on the above analysis from Table 1, and Figs. 1–6, the contribution of banana peel to MWBC surface area was demonstrated to be other types of surface area having greater adsorption action for metal ions, instead of porous surface area. The adsorption of MWBC for heavy metal ions probably mainly relied on much more adsorption sites on the large surface and quick transmission of heavy metal ions through the macro-porous and trench-like structures, and its pore adsorption only gave auxiliary effect. Some complex reaction appeared between the raw materials to form MWBC. The chemical absorption behavior performed by hydrogen bond and hydroxyl in MWBC was far stronger than that in H-MWBC. The adsorption mechanism of MWBC was basically dominated by chemical adsorption (that is, electrostatic neutralization/adsorption), assisted by physical adsorption of surface complexation and co-precipitation, while the adsorption mechanism of H-MWBC was mainly dominated by physical behavior.

This work provides a feasible resource utilization way for huge yields and extremely low utilization of banana peel and also provides a possibility for solving the phenomenon of sludge flooding China cities to a certain extent. In short, this work explores a feasible and realistic idea for recycling these two solid wastes and making biochars for removing heavy metals.

4. Conclusions

MWBC almost had no micropore structures. The surface of MWBC consisted of –OH, –O, and a small amount of –H, –N, –Si, $–NH_2$, and MWBC were a negatively charged carbon skeleton mainly composed of hydroxyl groups. The surface morphology of MWBC was mainly composed of more disordered structures, less pore structures and sheet structures, and planar structures, in which many disordered ditch-like structures having larger diameters were distributed. The zeta potential of MWBC was –80 – –10 mV, most of which concentrating around –60 – –40 mV, and there were more particles negatively large potential. The zeta potential of MWBC after adsorbing heavy metals shifted to the right.

The preferred pH for MWBC to adsorb Pb(II), Cu(II) and Zn(II) was 2, 4 and 4, in which the adsorption capacity reached 40.1, 40 and 39.6 mg/g at dosage 5 g/L, respectively, all the adsorption efficiency reaching 100%. The adsorption rate of MWBC for the three metal ions was Cu(II) > Zn(II) > Pb(II). MWBC appeared to be more sensitive to the temperature of Pb(II) solution than that of Cu(II) and Zn(II). When adsorbing Pb(II) and Cu(II) by MWBC, dosage and metal concentration ranges should be considered, but only metal concentration for Zn(II). The adsorption performance of MWBC for Cu(II) was higher than that of raw material BC. The adsorption effect of MWBC for metal ions was far higher than that of H-MWBC.

The adsorption of MWBC for Pb(II), Cu(II) and Zn(II) can be attributed to the pseudo-second-order kinetic process, and their equilibrium adsorption capacity were more closer to the actual adsorption capacity.

MWBC was a complex combination of sludge and banana peel, and some complex changes took place in MWBC structures. The contribution of banana peel to the surface area of MWBC was not manifested in the porous surface, but giving a positive effect on MWBC adsorption. The disordered structures gave more adsorption sites than the pore structures in MWBC and the higher adsorption for metal ions by MWBC resulted from more adsorption sites on the larger surface and rapid transportation of metals ions through the disordered structures. Having both hydrophilic

and hydrophobic properties, MWBC adsorption was a type of non-porous adsorption, showing the adsorption mechanism of chemical adsorption involving electrostatic neutralization/adsorption, supplemented by physical adsorption, and giving the strongest chemical adsorption for Zn(II) and stronger physical adsorption for Cu(II).

Acknowledgements

We acknowledge and thank the supporters from Shuifa Technology Group Co., Ltd (Setting up the Research Center of Shuifa Technology Group, University of Jinan), Shandong Province enterprise technology innovation project from Department of Industry and Information Technology of Shandong Province (202150100867) and University-enterprise joint project (w2021125).

References

[1] F. Benassi, S. Cividino, P. Cudlin, A. Alhuseen, G.R. Lamonica, L. Salvati, Population trends and desertification risk in a Mediterranean region, 1861–2017, Land Use Policy, 95 (2020) 104626, doi: 10.1016/j.landusepol.2020.104626.
[2] UNDDD, The United Nations Decade for Deserts (2010–2020) and the Fight Against Desertification, Bonn, Germany, 2017, Available at: http://www2.unccd.int/actions/united-nations-decade-deserts-2010–2020-and-fight-against-desertification
[3] O.A. Arojojoye, A.A. Oyagbemi, J.M. Afolabi, Toxicological assessment of heavy metal bioaccumulation and oxidative stress biomarkers in *Clarias gariepinus* from Igbokoda river of south western Nigeria, Bull. Environ. Contam. Toxicol., 100 (2018) 765–771.
[4] Y. Feng, Q. Bao, X. Xiao, M. Lin, Geo-accumulation vector model for evaluating the heavy metal pollution in the sediments of Western Dongting Lake, J. Hydrol., 573 (2019) 40–48.
[5] J.O. Nriagu, A history of global metal pollution, Science, 272 (1996) 223, doi: 10.1126/science.272.5259.223.
[6] D.S. Malik, C.K. Jain, A.K. Yadav, Removal of heavy metals from emerging cellulosic low-cost adsorbents: a review, Appl. Water Sci., 7 (2017) 2113–2136.
[7] F.-J. Zhao, Y. Ma, Y.-G. Zhu, Z. Tang, S.P. McGrath, Soil contamination in China: current status and mitigation strategies, Environ. Sci. Technol., 49 (2015) 750–759.
[8] Y. Du, L. Chen, P. Ding, L.L. Liu, Q.C. He, B.Z. Chen, Y.Y. Duan, Different exposure profile of heavy metal and health risk between residents near a Pb-Zn mine and a Mn mine in Huayuan county, South China, Chemosphere, 216 (2019) 352–364.
[9] K.H. Vardhan, P. Senthil Kumar, R.C. Panda, A review on heavy metal pollution, toxicity and remedial measures: current trends and future perspectives, J. Mol. Liq., 290 (2019) 111197, doi: 10.1016/j.molliq.2019.111197.
[10] A.D. Gupta, K.P. Rawat, V. Bhadauria, H. Singh, Recent trends in the application of modified starch in the adsorption of heavy metals from water: a review, Carbohydr. Polym., 269 (2021) 117763, doi: 10.1016/j.carbpol.2021.117763.
[11] P.N. Diagboya, B.I. Olu-Owolabi, F.M. Mtunzi, K.O. Adebowale, Clay-carbonaceous material composites: towards a new class of functional adsorbents for water treatment, Surf. Interfaces, 19 (2020) 100506, doi: 10.1016/j.surfin.2020.100506.
[12] P.N.E. Diagboya, E.D. Dikio, Silica-based mesoporous materials; emerging designer adsorbents for aqueous pollutants removal and water treatment, Microporous Mesoporous Mater., 266 (2018) 252–267.
[13] Y.W. Zhou, S.Y. Qin, S. Verma, T. Sar, S. Sarsaiya, B. Ravindran, T. Liu, R. Sindhu, A.K. Patel, P. Binod, S. Varjani, R.R. Singhnia, Z.Q. Zhang, M.K. Awasthi, Production and beneficial impact of biochar for environmental application: a comprehensive review, Bioresour. Technol., 337 (2021) 125451, doi: 10.1016/j.biortech.2021.125451.
[14] R.E. Ampiaw, W. Lee, Persimmon tannins as biosorbents for precious and heavy metal adsorption in wastewater: a review, Int. J. Environ. Sci. Technol., 17 (2020) 3835–3846.
[15] S. Papari, K. Hawboldt, R. Helleur, Pyrolysis: a theoretical and experimental study on the conversion of softwood sawmill residues to bio oil, Ind. Eng. Chem. Res., 54 (2015) 605–611.
[16] K.Z. Benis, A.M. Damuchali, J. Soltan, K.N. McPhedran, Treatment of aqueous arsenic – a review of biochar modification methods, Sci. Total Environ., 273 (2020) 111126, doi: 10.1016/j.jenvman.2020.111126.
[17] S. Yavari, M. Abualqumboz, N. Sapari, H.-A. Hata-Suhaimi, N.-Z. Nik-Fuaad, S. Yavari, Sorption of imazapic and imazapyr herbicides on chitosan-modified biochars, Int. J. Environ. Sci. Technol., 17 (2020) 3341–3350.
[18] X. Liu, H.Y. Nan, Q. An, The *Erythrina variegate* biochar's adsorption to NH_4^+–N and P from aqueous solution, J. Agric. Resour. Environ., 35 (2018) 66–73 (in Chinese).
[19] IBI Biochar Standards Version 2.0, Standardized Product Definition and Product Testing Guidelines for Biochar that is Used in Soil, The International Biochar Initiative, 2014. Available at: http://www.biochar-international.org/characterization-standard; https://www.biochar-international.org/wp-content/uploads/2018/04/IBI_Biochar_Standards_V2.1_Final.pdf (accessed on 23 November 2015).
[20] J. Lehmann, S. Joseph, Biochar for Environmental Management: Science, Technology and Implementation, 2nd ed., Routledge, London, 2015. Available at: http://doi.org/10.4324/9780203762264 (accessed on 4 March 2015).
[21] M. Inyang, E. Dickenson, The potential role of biochar in the removal of organic and microbial contaminants from potable and reuse water: a review, Chemosphere, 134 (2015) 232–240.
[22] A.U. Rajapaksha, S.S. Chen, D.C.W. Tsang, M. Zhang, M. Vithanage, S. Mandal, B. Gao, N.S. Bolan, Y.S. Ok, Engineered/designer biochar for contaminant removal/immobilization from soil and water: potential and implication of biochar modification, Chemosphere, 148 (2016) 276–291.
[23] J.Y. Tang, L.H. Zhang, J.C. Zhang, L.H. Ren, Y.Y. Zhou, Y.Y. Zheng, L. Luo, Y. Yang, H.L. Huang, A.W. Chen, Physicochemical features, metal availability and enzyme activity in heavy metal-polluted soil remediated by biochar and compost, Sci. Total Environ., 701 (2020) 134751, doi: 10.1016/j.scitotenv.2019.134751.
[24] W. Xiang, X.Y. Zhang, J.J. Chen, W.X. Zou, F. He, X. Hu, D.C.W. Tsang, Y.S. Ok, B. Gao, Biochar technology in wastewater treatment: a critical review, Chemosphere, 252 (2020) 126539, doi: 10.1016/j.chemosphere.2020.126539.
[25] Y.L. Liu, J.F. Huang, H.J. Xu, Y.L. Zhang, T. Hu, W.Z. Chen, H.J. Hu, J.H. Wu, Y.T. Li, G.B. Jiang, A magnetic macro-porous biochar sphere as vehicle for the activation and removal of heavy metals from contaminated agricultural soil, Chem. Eng. J., 390 (2020) 124638, doi: 10.1016/j.cej.2020.124638.
[26] K.P. Lu, X. Yang, G. Gielen, N. Bolan, Y.S. Ok, N.K. Niazi, S. Xu, G.D. Yuan, X. Chen, X.K. Zhang, D. Liu, Z.L. Song, X.Y. Liu, H.L. Wang, Effect of bamboo and rice straw biochars on the mobility and redistribution of heavy metals (Cd, Cu, Pb and Zn) in contaminated soil, J. Environ. Manage., 186 (2017) 285–292.
[27] S.Y. Wang, J.H. Kwak, M.S. Islamd, M.A. Naeth, M.G. El-Din, S.X. Chang, Biochar surface complexation and Ni(II), Cu(II), and Cd(II) adsorption in aqueous solutions depend on feedstock type, Sci. Total Environ., 712 (2020) 136538, doi: 10.1016/j.scitotenv.2020.136538.
[28] T. Bandara, J.M. Xu, I.D. Potter, A. Franks, J.B.A.J. Chathurika, C.X. Tang, Mechanisms for the removal of Cd(II) and Cu(II) from aqueous solution and mine water by biochars derived from agricultural wastes, Chemosphere, 254 (2020) 126745, doi: 10.1016/j.chemosphere.2020.126745.
[29] D.V. Cuong, N.L. Liu, V.A. Nguyen, C.H. Hou, Meso/micropore-controlled hierarchical porous carbon derived from activated biochar as a high-performance adsorbent for copper removal, Sci. Total Environ., 692 (2019) 844–853.
[30] R.P. Mohubedu, P.N.E. Diagboya, C.Y. Abasi, E.D. Dikio, F. Mtunzi, Magnetic valorization of biomass and biochar of a

typical plant nuisance for toxic metals contaminated water treatment, J. Cleaner Prod., 209 (2019) 1016–1024.
[31] J. Zhang, M. Lu, J. Wan, Y. Sun, H. Lan, X. Deng, Effects of pH, dissolved humic acid and Cu^{2+} on the adsorption of norfloxacin on montmorillonite-biochar composite derived from wheat straw, Biochem. Eng. J., 130 (2018) 104–112.
[32] H. Arabyarmohammadi, A.K. Darban, M. Abdollahy, R. Yong, B. Ayati, A. Zirakjou, S.E.A.T.M. van der Zee, Utilization of a novel chitosan/clay/biochar nanobiocomposite for immobilization of heavy metals in acid soil environment, J. Polym. Environ., 26 (2017) 2107–2119.
[33] L.Y. Gao, J.H. Deng, G.F. Huang, K. Li, K.Z. Cai, Y. Liu, F. Huang, Relative distribution of Cd^{2+} adsorption mechanisms on biochars derived from rice straw and sewage sludge, Bioresour. Technol., 272 (2019) 114–122.
[34] L.B. Qin, X.M. Huang, Q. Xue, L. Liu, Y. Wan, *In-situ* biodegradation of harmful pollutants in landfill by sludge modified biochar used as biocover, Environ. Pollut., 258 (2020) 113710, doi: 10.1016/j.envpol.2019.113710.
[35] X.C. Chen, G.C. Chen, L.G. Chen, Y.X. Chen, J. Lehmann, M.B. McBride, A.G. Hay, Adsorption of copper and zinc by biochars produced from pyrolysis of hardwood and corn straw in aqueous solution, Bioresour. Technol., 102 (2011) 8877–8884.
[36] N. Li, M.L. Yin, D.C.W. Tsang, S.T. Yang, J. Liu, X. Li, G. Song, J. Wang, Mechanisms of U(VI) removal by biochar derived from *Ficus microcarpa* aerial root: a comparison between raw and modified biochar, Sci. Total Environ., 697 (2019) 134115, doi: 10.1016/j.scitotenv.2019.134115.
[37] M. Ahmad, D.H. Moon, M. Vithanage, A. Koutsospyros, S.S. Lee, J.E. Yang, S.E. Lee, C. Jeon, Y.S. Ok, Production and use of biochar from buffalo-weed (*Ambrosia trifida* L.) for trichloroethylene removal from water, J. Chem. Technol. Biotechnol., 89 (2014) 150–157.
[38] X.J. Hu, X.B. Zhang, H.H. Ngo, W.S. Guo, H.T. Wen, C.C. Li, Y.C. Zhang, C.J. Ma, Comparison study on the ammonium adsorption of the biochars derived from different kinds of fruit peel, Sci. Total Environ., 707 (2018) 135544, doi: 10.1016/j.scitotenv.2019.135544.
[39] T.A. Khan, A.A. Mukhlif, EA. Khan, Uptake of Cu^{2+} and Zn^{2+} from simulated wastewater using muskmelon peel biochar: isotherm and kinetic studies, Egypt. J. Basic Appl. Sci., 4 (2019) 236–248.
[40] S.S. Lam, R.K. Liew, C.K. Cheng, N. Rasit, C.K. Ooi, N.L. Ma, J.-H. Ng, W.H. Lam, C.T. Chong, H.A. Chase, Pyrolysis production of fruit peel biochar for potential use in treatment of palm oil mill effluent, J. Environ. Manage., 213 (2018) 400–408.
[41] Z.P. Wang, K. Liu, L. Xie, H.N. Zhu, S.B. Ji, X.Q. Shu, Effects of residence time on characteristics of biochars prepared via co-pyrolysis of sewage sludge and cotton stalks, J. Anal. Appl. Pyrolysis, 142 (2019) 104659, doi: 10.1016/j.jaap.2019.104659.
[42] Q.Q. Yin, M.T. Liu, H.P. Ren, Biochar produced from the co-pyrolysis of sewage sludge and walnut shell for ammonium and phosphate adsorption from water, J. Environ. Manage., 249 (2019) 109410, doi: 10.1016/j.jenvman.2019.109410.
[43] J.A. Serna-Jiménez, F. Luna-Lama, Á. Caballero, M. de los Á. Martín, A.F. Chica, J.Á. Siles, Valorisation of banana peel waste as a precursor material for different renewable energy systems, Biomass Bioenergy, 155 (2021) 106279, doi: 10.1016/j.biombioe.2021.106279.
[44] J.Q. Albarelli, R.B. Rabelo, D.T. Santos, M.M. Beppu, M.A.A. Meireles, Effects of supercritical carbon dioxide on waste banana peels for heavy metal removal, J. Supercrit. Fluids, 58 (2011) 343–351.
[45] M. Kończak, Y.Z. Gao, P. Oleszczuk, Carbon dioxide as a carrier gas and biomass addition decrease the total and bioavailable polycyclic aromatic hydrocarbons in biochar produced from sewage sludge, Chemosphere, 228 (2019) 26–34.
[46] Y. Xiao, A. Raheem, L. Ding, W.-H. Chen, X.L. Chen, F.C. Wang, S.-L. Lin, Pretreatment, modification and applications of sewage sludge-derived biochar for resource recovery – a review, Chemosphere, 287 (2022) 131969, doi: 10.1016/j.chemosphere.2021.131969.
[47] S.Y. Tao, S. Liang, X. Wu, H.J. Hou, W.B. Yu, K.K. Xiao, B.C. Liu, S.S. Yuan, J.P. Hu, J.K. Yang, Enhanced silicon bioavailability of biochar derived from sludge conditioned with Fenton's reagent and lime, Sci. Total Environ., 806 (2021) 150941, doi: 10.1016/j.scitotenv.2021.150941.
[48] N. Zhou, H. Chen, J. Xi, D. Yao, Z. Zhou, Y. Tian, X. Lu, Biochars with excellent Pb(II) adsorption property produced from fresh and dehydrated banana peels via hydrothermal carbonization, Bioresour. Technol., 232 (2017) 204–210.
[49] K.M. Lavanya, J.A.K. Florence, B. Vivekanandan, R. Lakshmipathy, Comparative investigations of raw and alkali metal free banana peel as adsorbent for the removal of Hg^{2+} ions, Mater. Today:. Proc., 2021, doi: 10.1016/j.matpr.2021.07.410.
[50] M. Natalia Piol, C. Dickerman, M. Pilar Ardanza, A. Saralegui, S.P. Boeykens, Simultaneous removal of chromate and phosphate using different operational combinations for their adsorption on dolomite and banana peel, J. Environ. Manage., 288 (2021) 112463, doi: 10.1016/j.jenvman.2021.112463.
[51] Y. Fu, X.J. Meng, N.N. Lu, H.L. Jian, Y. Di, Characteristics changes in banana peel coagulant during storage process, Int. J. Environ. Sci. Technol., 16 (2019) 7747–7756.
[52] Y. Fu, X.J. Meng, Corresponding relationship between microorganism propagation and coagulation behavior of a hybrid fruit-peel coagulant, Desal. Water Treat., 216 (2021) 326–337.
[53] H.L. Jian, Preparation and Performance of a Hybrid Fruit-Peel Coagulant, Master Thesis, University of Jinan, Jinan, 2019 (in Chinese).
[54] M.H. Tahir, Z. Zhao, J. Ren, T. Rasool, S.R. Naqvi, Thermokinetics and gaseous product analysis of banana peel pyrolysis for its bioenergy potential, Biomass Bioenergy, 122 (2019) 193–201.
[55] J. Havukainen, A. Saud, T.F. Astrup, P. Peltola, M. Horttanainen, Environmental performance of dewatered sewage sludge digestate utilization based on life cycle assessment, Waste Manage., 137 (2022) 210–221.
[56] S.C. Hua, Preparation of Mix Waste Biochar and Its Removal of Heavy Metals, Master Thesis, University of Jinan, Jinan, 2019 (in Chinese).
[57] Y.S. Ho, G. Mckay, The kinetics of sorption of divalent metal ions onto sphagnum moss peat, Water Res., 34 (2000) 735–742.
[58] L. Lu, Y. Lin, Q.W. Chai, S.Y. He, C.P. Yang, Removal of acenaphthene by biochar and raw biomass with coexisting heavy metal and phenanthrene, Colloids Surf., A, 558 (2018) 103–109.
[59] L. Verma, J.W. Singh, Synthesis of novel biochar from waste plant litter biomass for the removal of arsenic (III and V) from aqueous solution: a mechanism characterization, kinetics and thermodynamics, J. Environ. Manage., 248 (2019) 109235, doi: 10.1016/j.jenvman.2019.07.006.
[60] X.Z. Zhu, Y.N. Li, X.N. Wang, Machine learning prediction of biochar yield and carbon contents in biochar based on biomass characteristics and pyrolysis conditions, Bioresour. Technol., 288 (2019) 121527, doi: 10.1016/j.biortech.2019.121527.
[61] X. Cui, H. Hao, C. Zhang, Z. He, X. Yang, Capacity and mechanisms of ammonium and cadmium sorption on different wetland-plant derived biochars, Sci. Total Environ., 539 (2016) 566–575.
[62] P. Khawas, A.J. Das, S.C. Deka, Production of renewable cellulose nanopaper from culinary banana (Musa ABB) peel and its characterization, Ind. Crops Prod., 86 (2016) 102–112.
[63] S. Li, S. Harris, A. Anandhi, G. Chen, Predicting biochar properties and functions based on feedstock and pyrolysis temperature: a review and data syntheses, J. Cleaner Prod., 215 (2019) 890–902.
[64] C.S. Kim, J.J. Rytuba, G.E.J. Brown, EXAFS study of Hg(II) sorption to Fe- and Al-(hydr)oxides: I. Effects of pH, J. Colloid Interface Sci., 271 (2004) 1–15.
[65] B. Tansel, J. Sager, T. Rector, J. Garland, R.F. Strayer, L. Levine, M. Roberts, M. Hummerick, J. Bauer, Significance of hydrated radius and hydration shells on ionic permeability during nanofiltration in dead end and cross flow modes, Sep. Purif. Technol., 51 (2006) 40–47.